Bone 49 (2011) 1357–1364

Contents lists available at SciVerse ScienceDirect

Bone

journal homepage: www.elsevier.com/locate/bone

Original Full Length Article

In vivo loading increases mechanical properties of scaffold by affecting bone formation and bone resorption rates

Alireza Roshan-Ghias [a], Floor M. Lambers [b], Mehdi Gholam-Rezaee [c], Ralph Müller [b], Dominique P. Pioletti [a,*]

[a] *Laboratory of Biomechanical Orthopedics, EPF Lausanne, Lausanne, Switzerland*
[b] *Institute for Biomechanics, ETH Zürich, Zürich, Switzerland*
[c] *CHUV, Lausanne, Switzerland*

ARTICLE INFO

Article history:
Received 7 July 2011
Revised 20 August 2011
Accepted 9 September 2011
Available online 18 September 2011

Edited by: Rene Rizzoli

Keywords:
Bone tissue engineering
Bone resorption
Mechanical stimulation
Finite element modeling
Micro-CT scanning

ABSTRACT

A successful bone tissue engineering strategy entails producing bone-scaffold constructs with adequate mechanical properties. Apart from the mechanical properties of the scaffold itself, the forming bone inside the scaffold also adds to the strength of the construct. In this study, we investigated the role of *in vivo* cyclic loading on mechanical properties of a bone scaffold. We implanted PLA/β-TCP scaffolds in the distal femur of six rats, applied external cyclic loading on the right leg, and kept the left leg as a control. We monitored bone formation at 7 time points over 35 weeks using time-lapsed micro-computed tomography (CT) imaging. The images were then used to construct micro-finite element models of bone-scaffold constructs, with which we estimated the stiffness for each sample at all time points. We found that loading increased the stiffness by 60% at 35 weeks. The increase of stiffness was correlated to an increase in bone volume fraction of 18% in the loaded scaffold compared to control scaffold. These changes in volume fraction and related stiffness in the bone scaffold are regulated by two independent processes, bone formation and bone resorption. Using time-lapsed micro-CT imaging and a newly-developed longitudinal image registration technique, we observed that mechanical stimulation increases the bone formation rate during 4–10 weeks, and decreases the bone resorption rate during 9–18 weeks post-operatively. For the first time, we report that *in vivo* cyclic loading increases mechanical properties of the scaffold by increasing the bone formation rate and decreasing the bone resorption rate.

Introduction

The accepted paradigm in bone tissue engineering is to combine a scaffold with cells and/or growth factors [1–6]. The scaffold is used for its osteoconductive properties [7,8] and the cells or growth factors are used for their osteoinductive or osteogenic properties [9,10]. While successful *in vivo* studies [11,12] and in clinical studies [13], this strategy has difficulties to settle in routine clinical practice. The reasons are manifold but often related to the cost, the stringent regulations established by the regulatory authorities, the specialized infrastructure needed, or the lack of possible reimbursement from health insurances when cells or growth factors are employed.

As the use of cells or growth factors is indeed the most difficult element to be included for bone tissue engineering, despite their acknowledged usefulness, we advocate a shift in the bone tissue engineering paradigm. Mechanical loading is an intrinsic stimulation present in the skeleton. It has been demonstrated in numerous *in vivo* studies to be correlated to bone regulation [14,15]. The in situ mechanical stimulation, if considered in an appropriate way, could then replace the cell and growth factor components of the bone tissue engineering strategy. This new paradigm has been proposed recently [16–18]. To support this approach, we have previously shown that controlled mechanical loadings on rat knee increase the bone volume fraction in polymeric scaffold implanted in the distal femur [19]. Indeed, bone adapts to mechanical stimulation by optimizing its mechanical properties [15], a process regulated by the interplay between bone formation and bone resorption [20].

Bone formation, through bone volume quantification, has generally been used to evaluate the *in vivo* scaffold performances [21–23]. Bone formation can be observed inside the scaffold as early as 1 week after implantation [24]. On the contrary, the aspects of bone resorption inside the scaffold have so far largely been neglected. Hing et al. [25] studied the effect of silicon level in silicate-substituted hydroxyapatite scaffold on bone formation and resorption using histological evaluations. It was observed that bone resorption inside the scaffold started 3 weeks after implantation. To our knowledge, quantitative measurements of the bone resorption rate inside the scaffold have so far not been reported.

In this study, we hypothesize that a short period of *in vivo* loading increases the mechanical properties of bone-scaffold constructs. We then hypothesize that loading affects not only the bone formation,

* Corresponding author at: EPFL/STI/IBI/LBO, Station 19, 1015 Lausanne, Switzerland. Fax: +41 21 693 86 60.
E-mail address: dominique.pioletti@epfl.ch (D.P. Pioletti).

8756-3282/$ – see front matter © 2011 Elsevier Inc. All rights reserved.
doi:10.1016/j.bone.2011.09.040

but also the bone resorption. We quantify the formation and resorption rates of the bone inside the scaffold longitudinally using *in vivo* time-lapsed micro-computed tomography (micro-CT).

Materials and methods

Surgery

Both distal femurs of 6 female Wistar rats of weight of 245–250 g were subjected to surgery (Veterinary Authority from the Canton of Vaud, authorizations no. 2140). Animals were anesthetized by Isoflurane, and Morphasol (Swissmedic, Bern, Switzerland) was injected as analgesia. In each leg, a hole of 3 mm in diameter and height was made using a metal drill bit on the lateral side of the distal femur underneath the growth plate. Afterwards, PLA/5wt.% β-TCP scaffolds (80% porous) [26] of the same size were implanted inside the holes [10]. No cells or growth factors were added in the scaffold. The scaffolds were perfused with PBS prior to implantation to remove the air bubbles.

In vivo loading

The loading started 2 weeks after the surgery. The animals were kept under anesthesia by Isoflurane during the loading session. The right knee joint of all animals was loaded in the anterio-posterior direction by loading the tibia axially. The left leg was kept as control. Compressive load of 10 N at 4 Hz for 5 min was applied by a custom-made machine used in previous studies [19,27]. The magnitude of loading was chosen in a way that animals don't show any sign of pain using their loaded joint after recovery. The animals were loaded every other day resulting in a total of 5 loading sessions being spread out over 10 days. For the remainder of the study, the bone-scaffold constructs were left without a loading intervention.

In vivo micro-CT imaging

Both knee joints of all animals were longitudinally scanned at 7 time points (2, 4, 7, 11, 15, 22 and 35 weeks after surgery) using a SkyScan 1076 *in vivo* scanner (SkyScan, Kontich, Belgium). Each leg was stretched to separate it from the body and scanned along with two phantoms (Gloor Instruments, Uster, Switzerland) and a tube of water. The same parameters were kept identical for all scans (18 μm, 80 kV, 124 μA, 1 mm Al filter, 600 ms exposure time). Reconstruction and analysis were done using NRecon and CTan software (SkyScan, Kontich, Belgium), respectively. The region of interest (ROI) was selected as a cylinder fitting inside the hole, starting 1 mm from the drill tip mark in the bone close to the cortical bone surface. Bone mineral density (BMD) value of 0.5 g/cm^3 was used to threshold bone. Scaffold was not visible in the images due to the low absorption values of PLA. TCP particles were too small to be detected with the resolution used. Accordingly, bone volume fraction (BV/TV) and BMD of the bone tissue were measured. Furthermore, connectivity density (Conn.D), trabecular thickness (Tb.Th), trabecular separation (Tb.Sp), and trabecular number (Tb.N) were quantified at all time points in accordance with the guidelines for the assessment of bone microstructure in rodents using micro-CT [28].

Dynamic bone morphometry

Calculation of the dynamic bone morphometry parameters was based on the fact that we had time-lapsed consecutive images that could be registered to the previous time point. Thus, differences in bone formation and resorption could be visualized and quantified as described earlier [29]. In short, the gray-scale CT data at week 2 served as baseline, while follow-up image data were always registered on the previous time point, i.e. week 4 on week 2 (2–4), week 7 on week 4 (4–7), etc. Afterwards, by adding (gauss-filtered, thresholded) follow-up measurements, sites of bone formation (only present in second time point), bone resorption (only present in first time point), or quiescent sites (present at both time points) could be visualized. A mask was defined which included the region of the scaffold present at all time points, such that only bone formation and resorption would be captured (and not because of e.g. missing slices). Within this mask, 3D dynamic bone morphometry parameters were calculated according to [29]. Bone formation rate (BFR) with the unit [%/day], was defined as the volume of bone formed between time points, divided by the total volume of the mask, divided by the time between scans. Similarly, the bone resorption rate (BRR) with the unit [%/day], was defined as the volume of resorbed bone per total volume of the mask, per time between scans. The following parameters were defined accordingly to a previous work [29]. Mineral apposition rate (MAR) was the mean thickness of formation packets, divided by the number of days between measurements, with unit [μm/day]. Likewise, mineral resorption rate (MRR) represented the mean depth of resorption pits, per time between measurements, with unit [μm/day]. Mineralizing surface (MS) was calculated as the surface of the formed bone, divided by the bone surface at the initial bone surface of the overlay, reported in percentage. Correspondingly, eroded surface (ES) was calculated by dividing the resorbed bone surface by the bone surface of the earlier time points, reported in percentage.

Finite element modeling

The micro-CT images of all samples were used to evaluate the Young's modulus (E) of bone-scaffold construct over time. To reduce computational cost, images inside the ROI were resampled to have a pixel size of 55 μm. Images were converted to finite element meshes, considering each voxel a hexahedral element using Matlab (Mathworks, Natick, USA). A modified gray-value voxel conversion technique [30] was used to obtain mechanical properties of each element. In short, the gray value (GV) of each voxel was converted to a value between 0 and 1. To this end, the minimum threshold was set to be the lowest GV that can be considered as mineralized tissue. GV below this threshold was set to zero. Accordingly, maximum threshold was set to be GV of the surrounding cortical bone. GV above this threshold was set to one. All elements were given isotropic linear elastic material properties with a Poisson's ratio of 0.3. The Young's modulus was based on the GV of elements:

$$E_{Element} = \left(E_{bone} - E_{Scaffold}\right) \cdot \left(GV_{Element}\right)^{\gamma} + E_{Scaffold}. \quad (1)$$

Where E_{bone} and $E_{Scaffold}$ are the Young's moduli of bone and scaffold, respectively. γ represents the underlying architecture of the element. The value of E_{Bone} is assumed to be 5 GPa and the value of γ was set at 1.5 following Homminga et al. [30]. The value of $E_{Scaffold}$ was measured previously to be 50 MPa [31]. In this model, we assumed that elements are either scaffold ($GV = 0$), forming bone ($0 < GV < 1$), or fully mature bone ($GV = 1$). The effect of degradation on architecture and mechanical properties of scaffold was neglected as 2 orders of magnitude separate the mechanical properties of the scaffold and the bone. The mesh was then exported to ABAQUS (Simulia, Providence, USA) for structural analysis. All degrees of freedom of nodes at the bottom of the scaffold were constrained. Axial degrees of freedom of top nodes were coupled together, and infinitesimal strain of 2% was applied on them. Direct sparse solver was used to solve the static structural problem, and by calculating reaction force at the top nodes, the Young's modulus of the constructs was calculated.

Histology

At the end of the study, the animals were euthanized, distal femurs were harvested and fixed with 4% paraformaldehyde, dehydrated using

graded ethanol series, cleared in Toluene, and embedded in resin. The bone was cut along the coronal plane into sections of 100 μm in thickness, and was then sanded to 50 μm slides. Safranin O staining was used to differentiate bone, soft tissue, and scaffold.

Statistical analysis

Generalized Additive Mixed Model (GAMM) was used to model and test the effect of loading for all parameters [32]. A separate GAMM was fitted to the measured parameters of each group. The predicted value of each parameter was compared between both groups. To test the difference between the loaded and control groups at each time point, *t*-test was performed between the predicted values of each group. All statistical analyses were done in R [33].

To find the best combination of bone morphometric parameters describing the Young's modulus, we fitted a generalized additive mixed model to all possible models, and extracted the adjusted R-squared of each fitted model. Each model was a linear combination of 1 to 6 bone morphometric parameters. The adjusted R-squared can be interpreted as the proportion of explained variance in a model, and is widely used as an indicator of a model's prediction power [34].

Results

Biomechanical analysis

The structure of the bone formed inside the scaffold (Fig. 1a). Fig. 1b shows the distribution of strain inside the scaffold. The strain was markedly lower in the bone compared to the pore space and it increased toward the center of the pores.

Fig. 2 shows that apparent Young's modulus of bone-scaffold constructs had an s-shaped curve over time. The control group had an inflection point at around 12 weeks, while in the loaded group the inflection point occurred sooner, at 9 weeks. We also observed that the loaded group had significantly higher mechanical properties compared to the control group from 5 weeks onward. At 35 weeks, the Young's modulus of the loaded group was 60% higher than the control group (p-value<0.001).

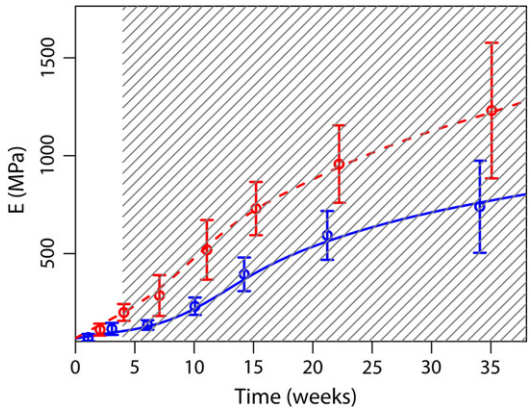

Fig. 2. Young's modulus of bone-scaffold constructs. The data are shown as average and 95% confidence interval of the average. The lines represent the fitted GAMM model. The control group is in solid blue line, and the loaded group is in dashed red line. The hatched rectangle shows the time span where a significant difference exists between the two groups.

Bone morphometry

Bone formation inside the scaffold started as early as 2 weeks. In both groups, we observed a gradual increase in the bone volume inside the scaffold up to the last measurement point (35 weeks). BV/TV increased almost linearly until 15 weeks, but it gradually reached a plateau at the last two measurement points (Fig. 3a). The loading had a significant effect on BV/TV from 7 weeks onwards, resulting in 18% higher BV/TV in the last time point compared to the control group (p-value<0.001). BMD also increased with time, as an indication of maturation of bone tissue (Fig. 3b). However, loading had no significant effect on BMD. Conn.D increased up to 15 weeks but then started to decline in both groups (Fig. 3c). The effect of loading on Conn.D was significant from 6 to 21 weeks. Tb.Th increased with time, but it was not significantly different between the two groups except at the last time point (Fig. 3d). On the contrary, Tb.Sp decreased in time in both groups and the effect of loading was significantly different only between 4 and 8 weeks (Fig. 3e). Tb.N increased initially, but reached a plateau at the later measurement times (Fig. 3f). The effect of loading on Tb.N was significant from 5 weeks until the last measurement.

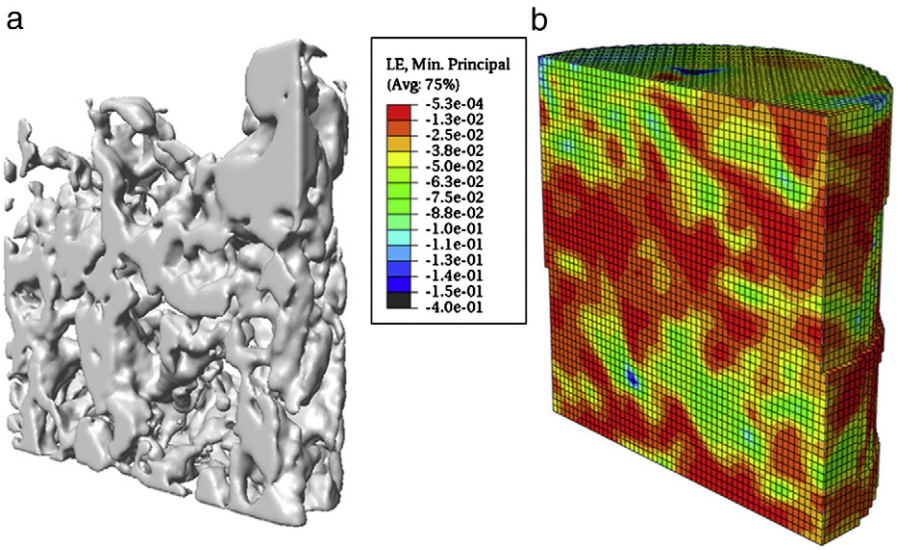

Fig. 1. (a) 3D reconstruction of bone in a scaffold at 15 weeks (control group), (b) Minimum principle strain distribution inside the same bone-scaffold construct. The low values of strain represented in red, mostly follows the bone structure.

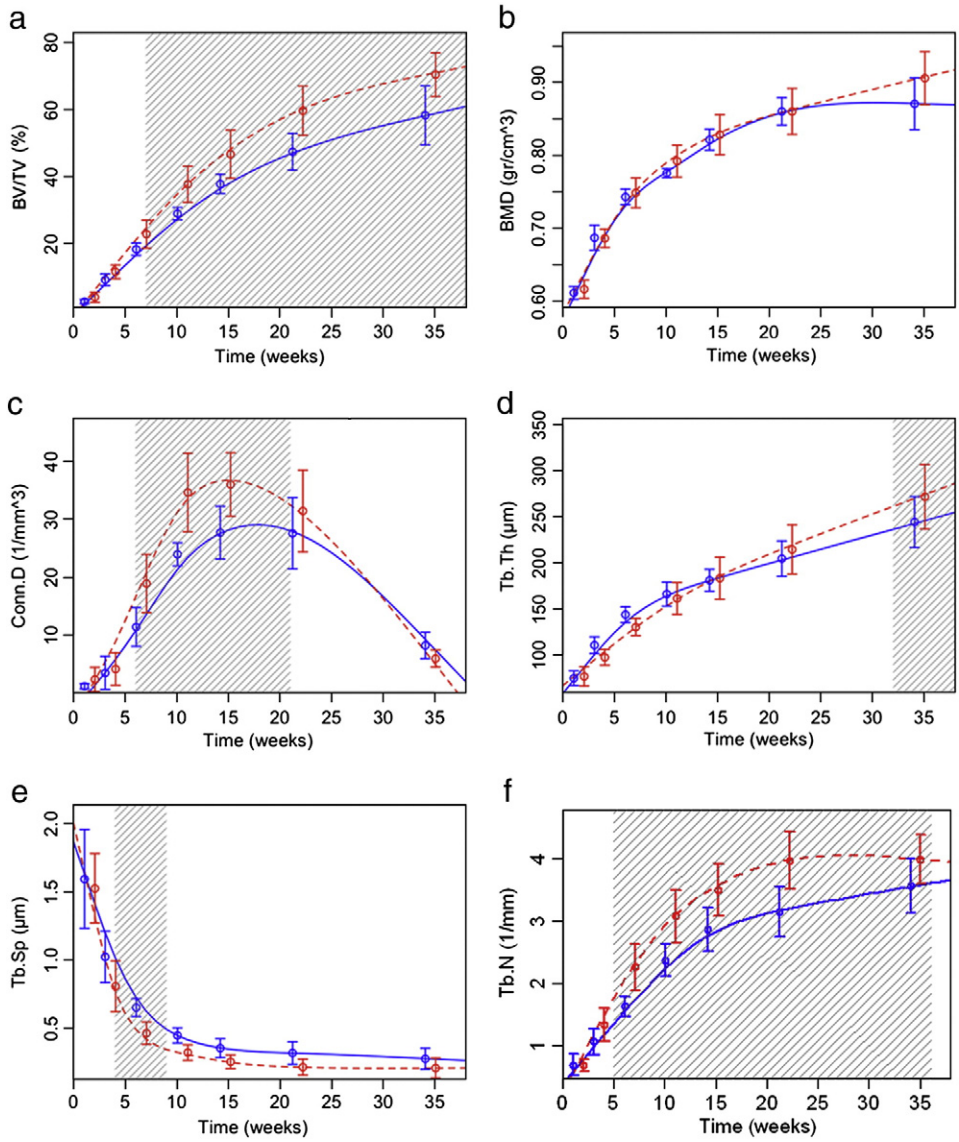

Fig. 3. Evolution of (a) BV/TV, (b) BMD, (c) Conn.D, (d) Tb.Th, (e) Tb.Sp, and (f) Tb.N, over time. The hatched rectangles show the time span where a significant difference exists between the two groups (p-value<0.05). The control group is in solid blue line, and the loaded group is in dashed red line.

Relations between stiffness and bone-scaffold morphometric parameters

Possible correlations between the mechanical and morphometry properties of the scaffold-bone constructs were evaluated. Table 1 shows different models of linear combination of morphometric parameters used to explain the variance of the Young's modulus with their corresponding adjusted R-squared values. The best adjusted R-squared belonged to the model with BV/TV, Conn.D, Tb.Th and Tb.N as explanatory variables, giving an adjusted R-squared of 0.93. However, BV/TV along with various combinations of Tb.Th, Tb.N and Conn.D also showed the same prediction power. Surprisingly, the model with BV/TV alone was also among the best models and gave an adjusted R-squared of 0.91. The improvement of the model with 3 more variables compared to the model with only BV/TV was almost negligible. It should be noted that no other single bone morphometric parameter was able to explain the variance in Young's modulus as well as BV/TV (Fig. 4).

Dynamic bone morphometry

Fig. 5 shows superimposed images of follow-up time points for a bone-scaffold construct in the loaded and control groups. For both loaded and control groups, the increase in bone volume fraction over time could be explained by the fact that bone formation always exceeded bone resorption. Nevertheless, BFR was significantly greater for the loaded compared to the control groups between 4 and 10 weeks (Fig. 6a). Bone resorption started from the early time points (between 2 and 4 weeks) and it continued until the last measurement. BRR, which was rather constant for the loaded group, was significantly smaller than the control group between 9 and 18 weeks (Fig. 6b). This

Table 1
Adjusted R-squared for different models explaining the variation in stiffness of the bone-scaffold construct.

	BV/TV Conn.D, Tb.Th Tb.N	BV/TV Conn.D Tb.N	BV/TV Conn.D Tb.Th	BV/TV Tb.Th Tb.N	BV/TV Tb.Th	BV/TV	Tb.N	Tb.Th	Tb.Sp	BMD	Conn.D
Adj.R^2	0.934	0.930	0.926	0.924	0.924	0.910	0.753	0.753	0.753	0.723	0.098

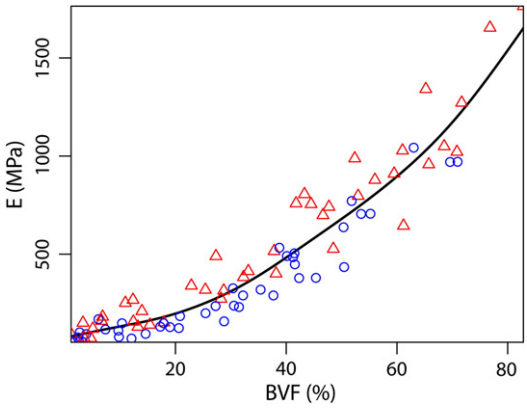

Fig. 4. The relation between Young's modulus and bone volume fraction. The control group is shown with blue circle, and the loaded group is shown with red triangles.

indicated that the loading had a beneficial effect on BV/TV by both increasing bone formation and decreasing bone resorption. When further investigating the shapes of formation/resorption sites, it was found that the thickness of formation and resorption sites gradually decreased over time (Fig. 6c and d). MAR was significantly smaller for loaded than control groups between 4 and 14 weeks (Fig. 6c), while MRR was significantly smaller in the loaded group between 6 and 16 weeks (Fig. 6d). On the other hand, when examining how much surface was occupied by formation/resorption sites, it was found that for both groups the surface percentage increased over time, and that the surface occupied by formation sites was about twice the surface taken up by resorption sites (Fig. 6e and f). MS was significantly greater for loaded than control groups from week 5 until the end of the study (Fig. 6e). On the contrary, ES was significantly smaller for loaded than control groups between week 7 and 21 (Fig. 6f). This indicates that loading mostly had an effect on the surface area occupied by the formation/resorption sites rather than their thickness.

Histology

In the region where around the walls of the pores and there was bone marrow in the pores, much like the trabecular bone. In the region where the scaffold was in contact to a cortical bone, however, we observed that the pores were completely filled with bone, similar to the cortical bone (Fig. 7). The scaffold was still present after 8 months of implantation. The scaffold was present in all samples and no signs of degradation could be observed. We did not compare loaded and control groups using histology.

Discussion

At the onset of the study, we hypothesized that a short initial period of *in vivo* cyclic loading enhances the long-term mechanical properties of a bone-scaffold construct. To that end, we were able to demonstrate that the initial loading increased the apparent Young's modulus and BV/TV of the bone-scaffold construct by 60% and 18% respectively at 35 weeks as compared to the control group. The increase in BV/TV due to loading was the result of an increase in bone formation rate and a decrease in bone resorption rate. The increase in scaffold mechanical properties when loading is applied has been previously shown but only with scaffolds containing recombinant human bone morphogenetic protein 2 [17] or mesenchymal stem cells [16]. The results obtained in the present study open the possibility to adapt the general paradigm in bone tissue engineering by replacing cells and growth factors with mechanical stimulation as the only additional osteogenic factor. Obviously, this would be possible only if the mechanical stimulation can be controlled. The mechanical stimulation protocol would then need to be carefully defined.

In a previous study, loading starting 3 days after the scaffold implantation resulted in an initial decrease in BV/TV [19]. In the present study, we increased the delay to 2 weeks as we hypothesized that the initial negative effect was because of the early loading. We verified our hypothesis and did not observe an initial decrease in BV/TV when loading started 2 weeks after implantation. Nevertheless, comparing the bone formation rate between the early and late loading study, we observed that the early loading study resulted in a higher BFR than late loading study (data not shown). Therefore, a trade-off between early and late loading has to be determined to optimize the effect of loading on bone formation. Given the results of these two studies, we suggest that the best strategy is to avoid early loading and to start loading within 1 to 2 weeks after surgery.

Loading not only affected the amount of bone in the scaffold, a result already reported in the literature i.e. [17], but also influenced the architecture of newly formed bone inside scaffold as shown in the present study. Structural and mechanical properties being intimately correlated in bone [35], we then tried to relate the stiffness with bone morphometric parameters in the scaffold. We found that a combination of BV/TV, Conn.D, Tb.Th, and Tb.N can explain more than 93% of variation in stiffness. However, BV/TV alone could already explain 91% of the variation, implying that the other parameters are of second order in importance. This finding has been reported by others as well [35–37]. In particular, Kabel et al. [38] studied the effect of bone morphometric parameters on stiffness of the trabecular bone using

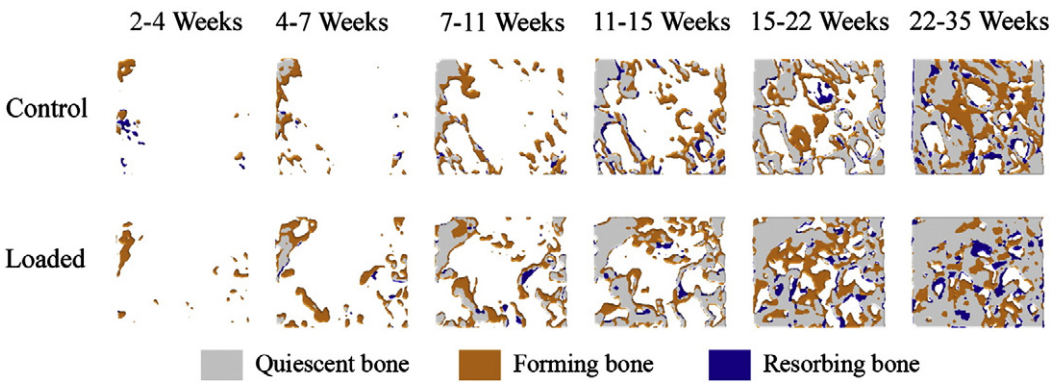

Fig. 5. Cross-section of time-lapsed overlaid scaffolds.

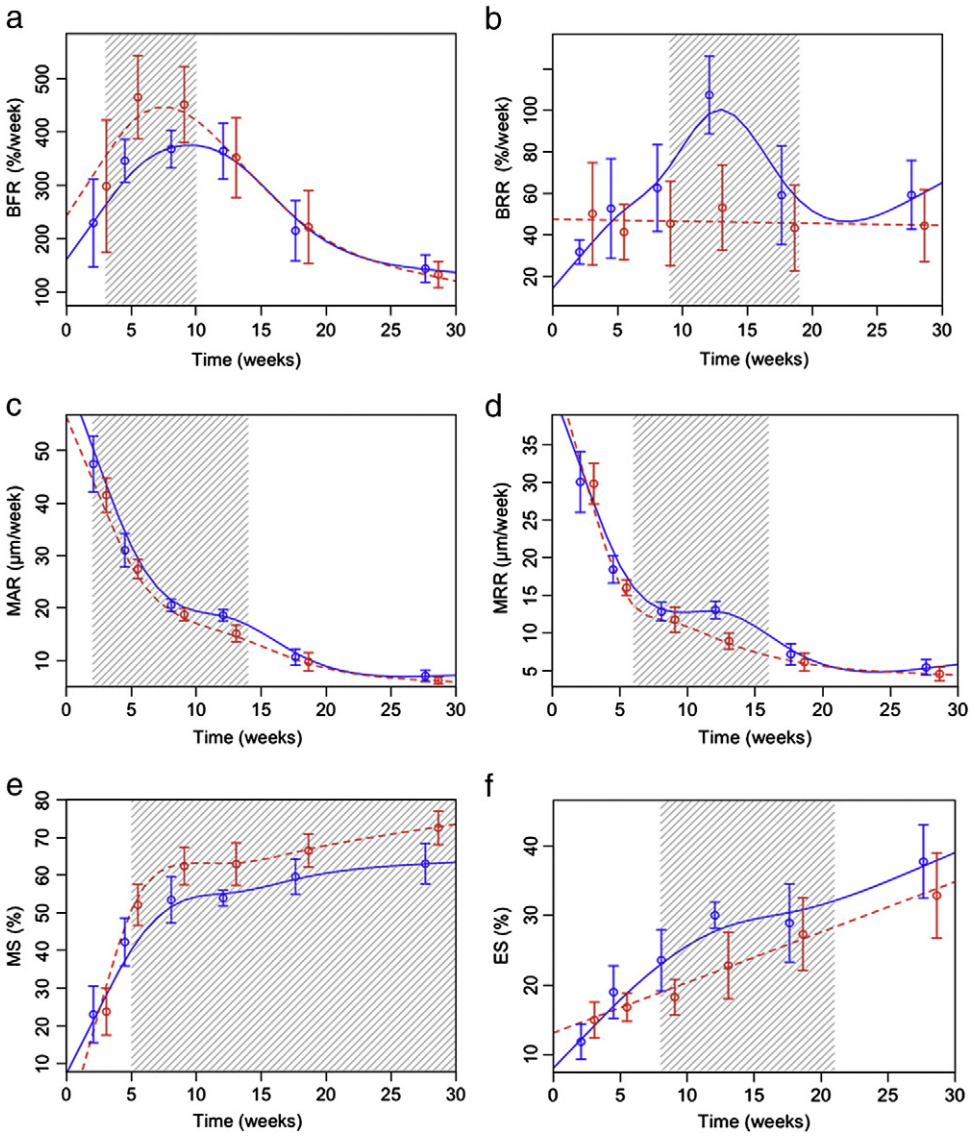

Fig. 6. Evolution of (a) BFR, (b) BRR, (c) MAR, (d) MRR, (e) MS, and (f) ES, over time. The hatched rectangles show the time span where a significant difference exists between the two groups. The control group is in solid blue line, and the loaded group is in dashed red line.

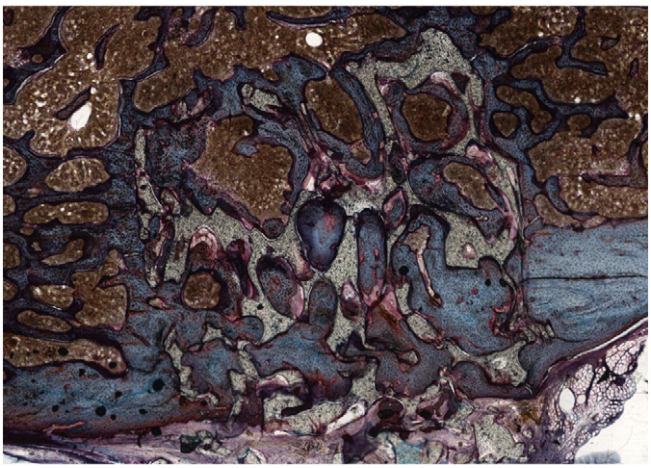

Fig. 7. A transverse cross-section of scaffold in the bone after 35 weeks (loaded group). Bone is in blue/green, scaffold is in gray and bone marrow is in brown.

micro-finite element analysis. They found that BV/TV explained by far the greatest part (84%–94%) of the variation in stiffness. When connectivity density and surface density were included, the correlations increased only marginally to 89%–95%.

Bone volume fraction is the result of two processes, bone formation and bone resorption. Thus, quantifying the effect of loading on these two processes could bring new information to optimize the effect of loading. Indeed, as demonstrated in this study, the possibility to calculate formation/resorption rates over time within the same scaffold is a clear advantage over destructive histology, which only allows single time point to be investigated per scaffold. Employing a technique previously developed and validated for studying remodeling in bone [29], we applied micro-CT-based dynamic 3D morphometry for the first time in these evolving bone-scaffold constructs to investigate the transient nature of bone formation/resorption. Furthermore, this technique also allowed the determination of the resorption rate, which is not directly accessible in dynamic histomorphometry. Using this analysis, we found that loading had a beneficial effect on the bone-scaffold construct, and acted both by increasing bone formation rate and by decreasing bone resorption rate. Interestingly, this effect was prominent by increasing the surface area

occupied by formation sites, and decreasing the surface taken up by resorption sites, while the thickness of formation packets, and the depth of resorption cavities were less affected. In studies where the bone was directly loaded, similar trends have been observed [39–41]. This indicates that analogous biological processes that cause bone to adapt to loading take place in the scaffold, even weeks after loading is finished.

A limitation in the calculation of formation/resorption rates was that the time spans between measurements differed and were relatively long for the later time points. The calculation of formation/resorption rates has been shown to be most sensitive for a time-span of 4 weeks between scans [29]. When rates are calculated from larger time intervals, intermediate formation/resorption is not captured, and leads to an underestimation of the rates.

Using trabecular architecture parameters (Tb.Th, Tb.Sp, and Tb.N) for the late time points is questionable, as the bone formed in the cortical region of the scaffold more and more resembled cortical bone (Fig. 7). Thus, the interpretation of the increase in Tb.Th in the loaded group at the last time point has to be considered with some caution.

The micro-finite element model used had some limitations. We assumed that anything other than the bone is scaffold, as we could not distinguish between scaffold and soft tissue using micro-CT imaging. To compensate for this assumption, we assigned the apparent mechanical properties of scaffold to all elements, i.e. we averaged the soft tissue and scaffold mechanical properties. This assumption does not affect the results significantly as the stiffness of the bone-scaffold constructs was mainly provided by bony tissues. Moreover, in order to determine the mechanical properties of the bone, we modified the method proposed by Homminga et al. [30] for the determination of mechanical properties of a trabecular bone. However, no experimental study has been done to verify if this relation is valid for mechanical properties of the bone forming in the scaffold. Thus, in the absence of experimental data on mechanical properties of the forming bone, we modified the available relation for trabecular bone. We also did not consider the deterioration of mechanical properties of scaffold due to degradation. However, as we compared the two groups, we expect the degradation effects to actually cancel out. We can also note that the structure of the scaffolds seemed to be intact after 8 months of implantation (Fig. 7), though the mechanical properties of PLA might have deteriorated over time.

In conclusion, we found that 5 bouts of cyclic loading after 2 weeks of implantation enhanced the apparent Young's modulus of the bone-scaffold constructs by almost 60% after 35 weeks over the control. This increase in Young's modulus was correlated foremost to the increase in bone volume which was 18% greater than the bone volume in the control group at 35 weeks. We found this increase to be a direct consequence of both an increase in bone formation rate and a decrease in bone resorption rate in the loading group as compared to the control animals.

Acknowledgments

This project was supported by a SNSF grant (#205320-121893) and the Inter-Institutional Center for Translational Biomechanics EPFL-CHUV-DAL.

References

[1] Salgado AJ, Coutinho OP, Reis RL. Bone tissue engineering: state of the art and future trends. Macromol Biosci 2004;4:743–65.
[2] Street J, Bao M, de Guzman L, Bunting S, Peale Jr FV, Ferrara N, et al. Vascular endothelial growth factor stimulates bone repair by promoting angiogenesis and bone turnover. Proc Natl Acad Sci U S A 2002;99:9656–61.
[3] Richardson TP, Peters MC, Ennett AB, Mooney DJ. Polymeric system for dual growth factor delivery. Nat Biotechnol 2001;19:1029–34.
[4] Chu TMG, Warden SJ, Turner CH, Stewart RL. Segmental bone regeneration using a load-bearing biodegradable carrier of bone morphogenetic protein-2. Biomaterials 2007;28:459–67.
[5] Meinel L, Karageorgiou V, Fajardo R, Snyder B, Shinde-Patil V, Zichner L, et al. Bone tissue engineering using human mesenchymal stem cells: effects of scaffold material and medium flow. Ann Biomed Eng 2004;32:112–22.
[6] Montjovent MO, Burri N, Mark S, Federici E, Scaletta C, Zambelli PY, et al. Fetal bone cells for tissue engineering. Bone 2004;35:1323–33.
[7] Kujala S, Ryhanen J, Danilov A, Tuukkanen J. Effect of porosity on the osteointegration and bone ingrowth of a weight-bearing nickel–titanium bone graft substitute. Biomaterials 2003;24:4691–7.
[8] Hoshikawa A, Fukui N, Fukuda A, Sawamura T, Hattori M, Nakamura K, et al. Quantitative analysis of the resorption and osteoconduction process of a calcium phosphate cement and its mechanical effect for screw fixation. Biomaterials 2003;24:4967–75.
[9] Jukes JM, Both SK, Leusink A, Sterk LM, van Blitterswijk CA, de Boer J. Endochondral bone tissue engineering using embryonic stem cells. Proc Natl Acad Sci U S A 2008;105:6840–5.
[10] Montjovent MO, Mark S, Mathieu L, Scaletta C, Scherberich A, Delabarde C, et al. Human fetal bone cells associated with ceramic reinforced PLA scaffolds for tissue engineering. Bone 2008;42:554–64.
[11] Rai B, Oest ME, Dupont KM, Ho KH, Teoh SH, Guldberg RE. Combination of platelet-rich plasma with polycaprolactone-tricalcium phosphate scaffolds for segmental bone defect repair. J Biomed Mater Res A 2007;81:888–99.
[12] Gauthier O, Muller R, von Stechow D, Lamy B, Weiss P, Bouler JM, et al. In vivo bone regeneration with injectable calcium phosphate biomaterial: a three-dimensional micro-computed tomographic, biomechanical and SEM study. Biomaterials 2005;26:5444–53.
[13] Vacanti CA, Bonassar LJ, Vacanti MP, Shufflebarger J. Replacement of an avulsed phalanx with tissue-engineered bone. N Engl J Med 2001;344:1511–4.
[14] Goodship AE, Watkins PE, Rigby HS, Kenwright J. The role of fixator frame stiffness in the control of fracture healing. An experimental study. J Biomech 1993;26:1027–35.
[15] Turner CH. Three rules for bone adaptation to mechanical stimuli. Bone 1998;23:399–407.
[16] Duty AO, Oest ME, Guldberg RE. Cyclic mechanical compression increases mineralization of cell-seeded polymer scaffolds in vivo. J Biomech Eng 2007;129:531–9.
[17] Boerckel JD, Dupont KM, Kolambkar YM, Lin AS, Guldberg RE. In vivo model for evaluating the effects of mechanical stimulation on tissue-engineered bone repair. J Biomech Eng 2009;131:084502.
[18] Pioletti DP. Biomechanics in bone tissue engineering. Comput Methods Biomech Biomed Engin 2010;13:837–46.
[19] Roshan-Ghias A, Terrier A, Bourban PE, Pioletti DP. In vivo cyclic loading as a potent stimulatory signal for bone formation inside tissue engineering scaffold. Eur Cell Mater 2010;19:41–9.
[20] Goodship A, Cunningham J. Pathophysiology of functional adaptation of bone in remodeling and repair in vivo. In: Cowin S, editor. Bone mechanics handbook. CRC; 2001.
[21] Oest ME, Dupont KM, Kong HJ, Mooney DJ, Guldberg RE. Quantitative assessment of scaffold and growth factor-mediated repair of critically sized bone defects. J Orthop Res 2007;25:941–50.
[22] Karp JM, Sarraf F, Shoichet MS, Davies JE. Fibrin-filled scaffolds for bone-tissue engineering: an in vivo study. J Biomed Mater Res A 2004;71:162–71.
[23] Stevens MM, Marini RP, Schaefer D, Aronson J, Langer R, Shastri VP. In vivo engineering of organs: the bone bioreactor. Proc Natl Acad Sci U S A 2005;102:11450–5.
[24] Vehof JW, Takita H, Kuboki Y, Spauwen PH, Jansen JA. Histological characterization of the early stages of bone morphogenetic protein-induced osteogenesis. J Biomed Mater Res 2002;61:440–9.
[25] Hing KA, Revell PA, Smith N, Buckland T. Effect of silicon level on rate, quality and progression of bone healing within silicate-substituted porous hydroxyapatite scaffolds. Biomaterials 2006;27:5014–26.
[26] Mathieu LM, Montjovent MO, Bourban PE, Pioletti DP, Manson JA. Bioresorbable composites prepared by supercritical fluid foaming. J Biomed Mater Res A 2005;75:89–97.
[27] Stadelmann VA, Hocke J, Verhelle J, Forster V, Merlini F, Terrier A, et al. 3D strain map of axially loaded mouse tibia: a numerical analysis validated by experimental measurements. Comput Methods Biomech Biomed Engin 2009;12:95–100.
[28] Bouxsein ML, Boyd SK, Christiansen BA, Guldberg RE, Jepsen KJ, Muller R. Guidelines for assessment of bone microstructure in rodents using micro-computed tomography. J Bone Miner Res 2010;25:1468–86.
[29] Schulte FA, Lambers FM, Kuhn G, Muller R. In vivo micro-computed tomography allows direct three-dimensional quantification of both bone formation and bone resorption parameters using time-lapsed imaging. Bone 2011;48:433–42.
[30] Homminga J, Huiskes R, Van Rietbergen B, Ruegsegger P, Weinans H. Introduction and evaluation of a gray-value voxel conversion technique. J Biomech 2001;34:513–7.
[31] Mathieu LM, Mueller TL, Bourban PE, Pioletti DP, Muller R, Manson JAE. Architecture and properties of anisotropic polymer composite scaffolds for bone tissue engineering. Biomaterials 2006;27:905–16.
[32] Wood S. Generalized additive models: an introduction with R. Chapman and Hall/CRC; 2007.
[33] R.D.C. Team. R: a language and environment for statistical computing. Vienna, Austria: R Foundation for Statistical Computing; 2010.
[34] Montgomery D. Applied statistics and probability for engineers. Wiley; 2010.

[35] Pothuaud L, Van Rietbergen B, Mosekilde L, Beuf O, Levitz P, Benhamou CL, et al. Combination of topological parameters and bone volume fraction better predicts the mechanical properties of trabecular bone. J Biomech 2002;35:1091–9.
[36] Boutroy S, Van Rietbergen B, Sornay-Rendu E, Munoz F, Bouxsein ML, Delmas PD. Finite element analysis based on in vivo HR-pQCT images of the distal radius is associated with wrist fracture in postmenopausal women. J Bone Miner Res 2008;23:392–9.
[37] Pistoia W, van Rietbergen B, Lochmuller EM, Lill CA, Eckstein F, Ruegsegger P. Estimation of distal radius failure load with micro-finite element analysis models based on three-dimensional peripheral quantitative computed tomography images. Bone 2002;30:842–8.
[38] Kabel J, van Rietbergen B, Dalstra M, Odgaard A, Huiskes R. The role of an effective isotropic tissue modulus in the elastic properties of cancellous bone. J Biomech 1999;32:673–80.
[39] Chow JW, Jagger CJ, Chambers TJ. Characterization of osteogenic response to mechanical stimulation in cancellous bone of rat caudal vertebrae. Am J Physiol 1993;265:E340–7.
[40] Chambers TJ, Evans M, Gardner TN, Turner-Smith A, Chow JW. Induction of bone formation in rat tail vertebrae by mechanical loading. Bone Miner 1993;20:167–78.
[41] Lean JM, Jagger CJ, Chambers TJ, Chow JW. Increased insulin-like growth factor I mRNA expression in rat osteocytes in response to mechanical stimulation. Am J Physiol 1995;268:E318–27.